AD-775 423

GRUNEISEN DATA FROM THE FREE SURFACE VELOCITY OF THERMOELASTIC MATERIALS

R. B. Oswald, et al

Harry Diamond Laboratories
Washington, D.C.

May 1973

AD-775423

DOCUMENT CONTROL DATA - R & D

(Security classification of title, body of abstract and indexing annotation must be entered when the overall report is classified)

1 ORIGINATING ACTIVITY (Corporate author)	2a. REPORT SECURITY CLASSIFICATION
Harry Diamond Laboratories Washington, D.C. 20438	Unclassified
	2b. GROUP

3 REPORT TITLE

Gruneisen Data From the Free Surface Velocity of Thermoelastic Materials

4 DESCRIPTIVE NOTES (Type of report and inclusive dates)

Technical Report

5 AUTHOR(S) (First name, middle initial, last name)

R. B. Oswald   D. R. Schallhorn
F. B. McLean
     T. R. Oldham

6 REPORT DATE	7a. TOTAL NO. OF PAGES	7b. NO. OF REFS
May 1973	40 36	14
8a. CONTRACT OR GRANT NO	9a. ORIGINATOR'S REPORT NUMBER(S)	
b. PROJECT NO DA-1B062113A661	HDL-TR-1629	
c. AMCMS Code: 502N.11.07000	9b. OTHER REPORT NO(S) (Any other numbers that may be assigned this report)	
d. HDL Proj: 25227		

10 DISTRIBUTION STATEMENT

Approved for public release; distribution unlimited.

11 SUPPLEMENTARY NOTES	12. SPONSORING MILITARY ACTIVITY
Research sponsored by the Army Materials and Mechanics Research Center, Watertown, Mass.	AMMRC

13. ABSTRACT

A technique is presented for the measurement of the Gruneisen parameter (Γ) of a solid from the free surface velocity induced by pulsed energy deposition. The technique is used to obtain both temperature-dependent and temperature-independent Gruneisen data. The measurements employ a velocity interferometer to determine the free surface velocity of solids exposed to a pulsed electron beam. For the cases where Γ is independent of temperature, the Γ values are obtained from the maximum free surface velocity as a function of incident fluence. For the temperature-dependent case, Γ is extracted by an analysis based on the differentiation of the free surface velocity with respect to the initial temperature of the solid. The analysis takes into account the effects of both the finite exposure time of the electron pulses and the delay time of the interferometer. Results are presented for Al, Cu, Ge and Si in a temperature range where Γ is constant. In addition, Γ is measured for silicon as a function of temperature over the range 50°K to 300°K, where Γ is strongly temperature-dependent. In all cases the results are in excellent agreement with the thermodynamic values.

DD FORM 1473 REPLACES DD FORM 1473, 1 JAN 64, WHICH IS OBSOLETE FOR ARMY USE.

1

14 KEY WORDS	LINK A		LINK B		LINK C	
	ROLE	WT	ROLE	WT	ROLE	WT
Thermal shock						
Pulsed Electron Beam Exposure						
Impulse						
Blow-off						

1a

The findings in this report are not to be construed as an official Department of the Army position unless so designated by other authorized documents.

Citation of manufacturers' or trade names does not constitute an official indorsement or approval of the use thereof.

Destroy this report when it is no longer needed. Do not return it to the originator.

AD

HDL-TR-1629

GRÜNEISEN DATA FROM THE FREE SURFACE VELOCITY OF THERMOELASTIC MATERIALS

by

R.B. Oswald

F.B. McLean

D.R. Schallhorn

T.R. Oldham

May 1973

U.S ARMY MATERIEL COMMAND

HARRY DIAMOND LABORATORIES

WASHINGTON. D C 20438

1

ABSTRACT

A technique is presented for the measurement of the Grüneisen parameter (Γ) of a solid from the free surface velocity induced by pulsed energy deposition. The technique is used to obtain both temperature-dependent and temperature-independent Grüneisen data. The measurements employ a velocity interferometer to determine the free surface velocity of solids exposed to a pulsed electron beam. For the cases where Γ is independent of temperature, the Γ values are obtained from the maximum free surface velocity as a function of incident fluence. For the temperature-dependent case, Γ is extracted by an analysis based on the differentiation of the free surface velocity with respect to the initial temperature of the solid. The analysis takes into account the effects of both the finite exposure time of the electron pulses and the delay time of the interferometer. Results are presented for Al, Cu, Ge and Si in a temperature range where Γ is constant. In addition, Γ is measured for silicon as a function of temperature over the range 50°K to 300°K, where Γ is strongly temperature-dependent. In all cases the results are in excellent agreement with the thermodynamic values.

3

CONTENTS

FIGURES

Preceding page blank

CONTENTS (Continued)

I.   INTRODUCTION

When a solid is exposed to pulsed radiation, either photon or particle, the resulting rapid heating can generate thermoelastic stresses which then propagate through the medium. The magnitude of the thermo-elastic stress developed is characterized by the Grüneisen parameter Γ, which is defined in terms of thermodynamic parameters of the solid as $\Gamma = \beta/\rho K_T C_V$ where β is the volume coefficient of thermal expansion, ρ is the density, K_T is the isothermal compressibility, and C_V is the specific heat per unit mass at constant volume. The importance of Γ in describing the thermoelastic response of materials arises from the fact that Γ is directly related to the rate of change in pressure p with internal energy density E at constant volume:

$$\Gamma = \left(\frac{\partial p}{\partial E}\right)_V \tag{1}$$

For the case of pulsed energy deposition, the target sample can essentially be considered to be inertially clamped during the exposure time. Thus, if Γ is constant, the change in pressure $\Delta p(\vec{r})$ at the point $\vec{r}$ inside the sample due to an energy deposition $\Delta E(\vec{r})$ is $\Delta p(\vec{r}) = \Gamma\, \Delta E(\vec{r})$. More generally, if Γ is a function of temperature, or specific energy, the rise in pressure is given by

$$\Delta p(\vec{r}) = \int_{E_o}^{E_o + \Delta E(\vec{r})} \Gamma(E)\, dE \tag{2}$$

where E_o is the initial value of the internal energy density.

For most materials, Γ is fairly constant at room temperature and above, and their thermoelastic response at these temperatures is adequately char-acterized by a temperature-independent Grüneisen parameter. At lower temperatures, however, the variation of Γ with temperature often becomes significant. In some materials this variation is quite strong with Γ even becoming negative at sufficiently low temperature. Therefore, if one wishes to describe the thermoelastic response of these materials at low temperatures, it is necessary that the temperature dependence of Γ be known. In this paper we describe and demonstrate a technique that can be used to measure Γ as a function of temperature. The measurement is made by observing the free surface velocity induced by exposure to a pulsed electron beam.

It has been shown previously[1,2,3,4] that the thermoelastic response of solids can be utilized as a means of measuring Γ for solids char-acterized by a constant Γ. In particular, using a displacement type

[1] R. B. Oswald, Jr., D. R. Schallhorn, H. A. Eisen, and F. B. McLean, Appl. Phys. Letters 13, 270 (1968).

[2] R. B. Oswald, Jr., F. B. McLean, D. R. Schallhorn, and L. D. Buxton, Appl. Phys. Letters 16, 24 (1970).

[3] R. A. Graham and R. E. Hutchison, Appl. Phys. Letters 11, 69 (1967).

[4] R. B. Oswald, Jr., F. B. McLean, D. R. Schallhorn and L. D. Buxton, J. Appl. Phys. 42, 3463 (1971).

laser interferometer[3,4] to study free surface motion proved to be a fruitful and direct means of determining Γ. Displacement interferometry analysis was also applied to the study of the thermomechanical properties of certain materials at low temperatures.[5] It was found that introducing a one-dimensional thermoelastic model that explicitly accounts for the temperature dependence of Γ is indeed necessary for the description of the dynamic response of these materials. In this analysis the known temperature dependence of Γ as ascertained by thermal measurements of β, K_T, and C_V was used in comparing the experimental observations with the predictions of the thermoelastic model. No attempt was made to measure Γ(T) with the displacement interferometric technique, primarily because the reduction of displacement data to values for Γ requires the unfolding of a double integral and the resulting accuracy would be relatively poor.

The accuracy of the results for Grüneisen values is improved considerably if either induced stress or free surface velocity measurements are used, for then only a single integral is involved in the reduction of the data to Γ values. Gauster[6] recently employed a stress-gauge technique to relate Γ(T) with measured stress. In the present study we utilize a "velocity" interferometer of the type described by Barker[7] to measure the free surface velocity induced by a pulsed electron beam, and we describe the analysis for extraction of Γ(T). We note at the outset that the precision with which Γ can be measured by interferometric methods in general is of the order of 5%. This precision is certainly poorer than can be accomplished by careful thermodynamic measurements of β, K_T, and C_V. However, interferometric methods are direct, fast, and relatively simple, and yield results within the precision necessary for most engineering applications. Further, by averaging a number of data points, the precision is usually improved considerably.

In the next section we describe the analysis necessary to extract Grüneisen values from free surface velocity data. In essence, the analysis is a differential one, where the Grüneisen parameter is sampled only over limited regions of temperature, or internal energy density. Corrections for the finite duration of the electron pulse and for the delay time of the interferometer are included. In Section III we discuss the details of the experimental arrangement and procedures. In the final section, as a check on the technique, we first determine values of Γ for a number of materials over an energy interval where Γ is known and constant. We then use the technique to determine the temperature dependence of Γ by measuring Γ(T) for Si over a temperature interval from 50°K to 300°K, and compare our results with the results of thermal measurements.

[5]F. B. McLean, R. B. Oswald, Jr., D. R. Schallhorn and L. D. Buxton, J. Appl. Phys. 42, 3474 (1971).
[6]W. B. Gauster, Phys. Rev. B 4, 1288 (1971).
[7]L. Barker, Behavior of Dense Media Under High Dynamic Pressure, Symposium HDP IUTAM, Paris, 1967, Gordon and Breach, New York, N. Y. p. 483 (1968).

II. METHOD OF ANALYSIS

The measurement of the Grüneisen parameter presented here is based upon solutions of the one-dimensional thermoelastic equation of motion which include the dependence of Γ on the internal energy density[8], or temperature. These solutions have been described in detail previously;[4,5] thus, we briefly review only the results which pertain to the present discussion. We consider a thin slab of elastic material, initially at temperature T_o and corresponding specific energy E_o, exposed to a pulsed electron beam of uniform flux incident along the x axis. Let $x = 0$ denote the plane on which the beam is incident and $x = L$ denote the plane of the rear surface where velocity measurements are made. If the sample thickness is much smaller than the lateral dimensions, the central region of the sample will initially respond only along the x direction in a one-dimensional manner[9]. We therefore postulate that the deposited energy is immediately coupled to the lattice as thermal phonons and is characterized by an x-dependent deposition function $\Delta E(x)$ (with units energy per unit volume). Figure 1 shows a typical energy deposition profile, in this case for aluminum 6061 exposed to an electron spectrum with a mean energy of 1.96 MeV. Note that the energy deposition reaches its peak value a short distance x_p from the front surface. We take as a convenient measure of the electron beam exposure the energy deposition at the peak, $\Delta E_p = \Delta E(x_p)$. Also, we point out that for the present experiments the sample thickness L is always made greater than the electron range in the material; therefore, $\Delta E(x) \to 0$ for $x = L$. We assume that the temperature variations of the density, ρ, and of the acoustic speed, c, are small in comparison with the temperature variation of Γ and thus can be neglected. In addition, we assume that the electron pulse can be treated as a square wave in time of pulse width τ_o and we take $t = 0$ as the time the pulse first strikes the front surface of the sample. We further assume that attenuation of the stress pulse during the first cycle can be neglected or can be accounted for by a simple correction factor determined empirically.

In this paper we are interested in the motion of the rear surface, specifically the rear surface velocity, which from the results of reference 5 is given as a function of time by

$$V(L,t) \;=\; (1/\rho c \ell_o) \int_{L-ct}^{L-ct+\ell_o} dx\, K(x) \tag{3}$$

where $\ell_o = c\tau_o$ and $K(x)$ is defined by

$$K(x) \;=\; \int_{E_o}^{E_F(x)} \Gamma(E)\, dE \tag{4}$$

[8]W. B. Gauster, Phys. Rev. 187, 1035 (1969).
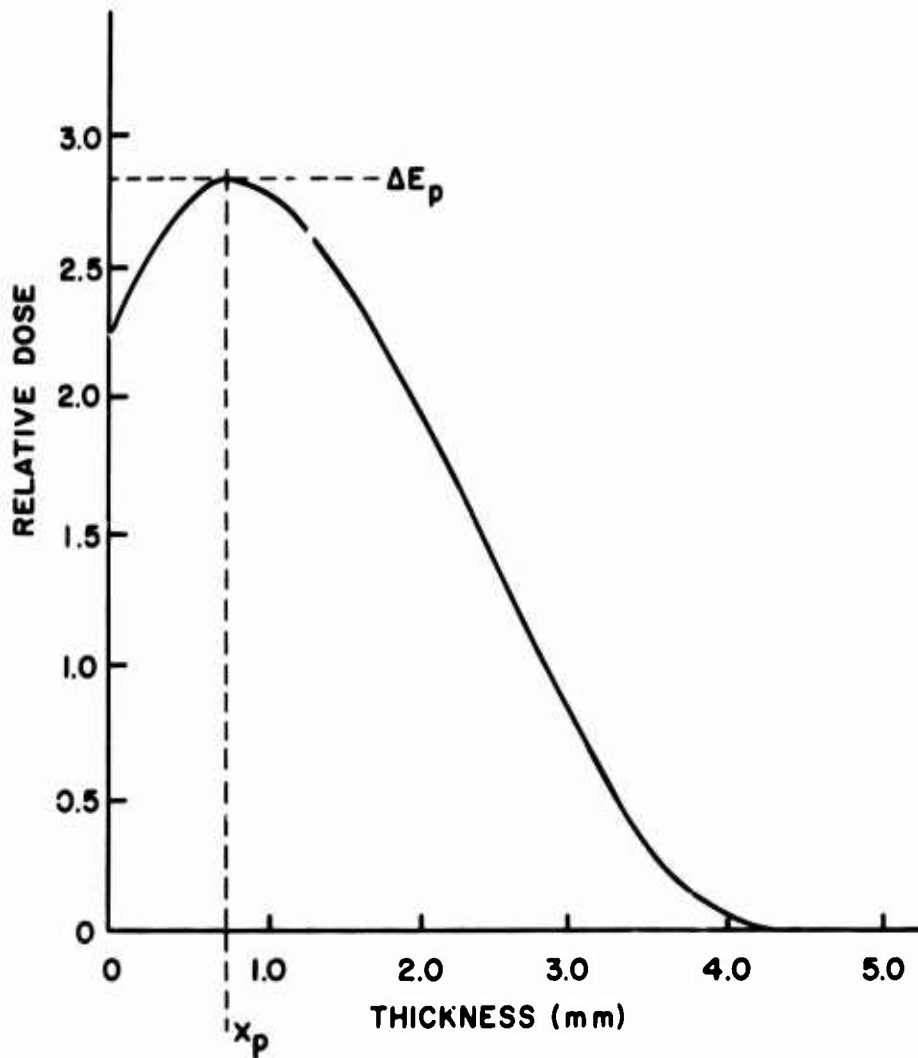[9]R. J. Clifton, J. Appl. Phys. 41, 5335 (1970).

Figure 1. Energy deposition profile in aluminum 6061 for the
1.96 MeV electron beam exposure.

for the range 0< x <L. To account for the periodic nature of the solu-
tion, the range of K(x) is extended to all x with K(x) being defined
for other values of x by the periodic conditions

$$K(-x) = -K(x)$$
$$K(x+2L) = K(x) \tag{5}$$
$$K(0) = 0$$

In Eq. (4) $E_F(x) = E_0 + \Delta E(x)$ is the final (x-dependent) energy density of the sample. The final temperature profile $T_F(x)$ is related to $E_F(x)$ by the expression

$$E_F(x) = \rho \int_{T_0}^{T_F(x)} C_V(T)dT \tag{6}$$

Eq. (3) gives the calculated velocity history of the rear surface as long as the stresses do not exceed the elastic limit of the material and attenuation is negligible.

Consider now what one is actually measuring with the velocity inter-ferometer. In particular, we must account for the effects of the finite rise time of the interferometer. In figure 2 we show a schematic[10] of the laser velocity interferometer (after ref 7). We follow the analysis given by Clifton.[9] Essentially, one is looking at the interference between two light beams One beam is reflected from the sample rear surface at time t and travels directly to the photomultiplier tube in time t_1 at the photomultiplier at time $t+t_1$. The other beam is reflected at time $t - \tau_D$ and is subjected to an optical delay of duration τ_D thus also arriving at the photomultiplier at time $t + t_1$. At time $t = 0$ the sample rear surface is stationary and we suppose that the two beam are adjusted so that they are in constructive interference, i.e., the delay leg is adjusted so that it contains an integer number of wavelengths λ. For $t > 0$ the rear surface begins to move, and the phases of the two light beams are shifted relative to each other, the phase shift being

$$\Delta\tau (t + t_1) = (2/C_L) \ |U(t) - U(t - \tau_D)| \tag{7}$$

where C_L is the speed of light and $U(t)$ is the displacement of the rear surface. We may drop the time t_1, as it merely shifts the entire time record by the constant value t_1. Now, every time the phase shift is equal to an integer times the period τ_L of the light waves, a fringe is detected by the photomultiplier tube—the two light beams are again in constructive interference. Thus, the fringe count $N(t)$ at time t is given by $N(t) = \Delta\tau(t)/\tau_L$ which, by (7) and rewriting the displacement as an integral over velocity, becomes

$$N(t) = (2/\lambda) \int_{t-\tau_D}^{t} V(t')dt' \tag{8}$$

This expression shows that the fringe count at time t is related to an "average" of the velocity over the time interval τ_D, centered around the time $t - \tau_D/2$. In fact, if τ_D is sufficiently small we can apply the mean value theorem to the integral in (8) to obtain

$$N(t) \cong 2\tau_0/\lambda \ V \ (t - \tau_D/2) \tag{9}$$

---

[10]M. J. Berger, in <u>Methods in Computational Physics</u>, edited by B. Alder, et al (Academic Press, New York, 1963), Vol. 1, p. 135.
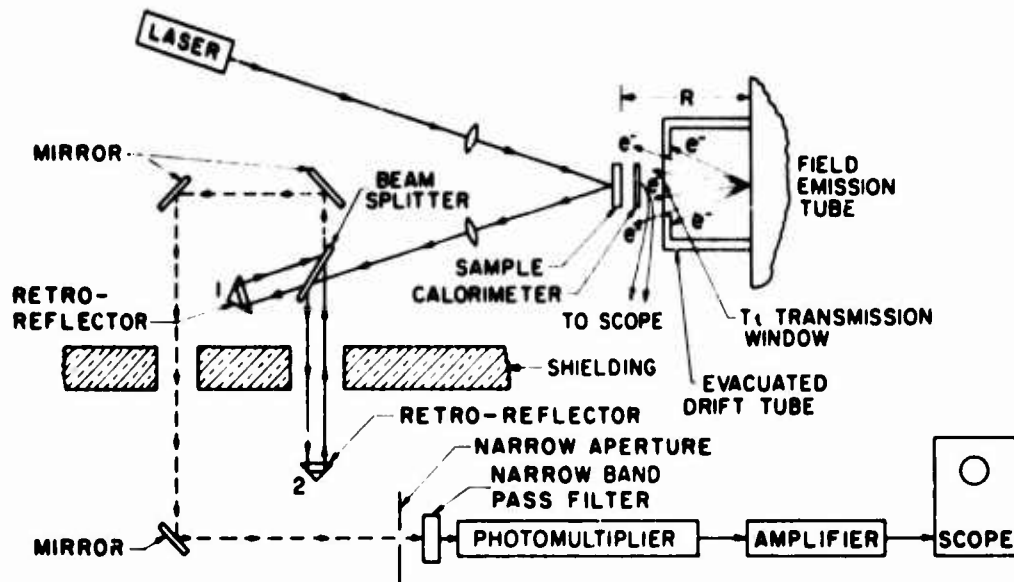
Figure 2. Schematic diagram of the experimental arrangement depicting the velocity interferometer, the sample, the calorimeter, and pulsed-electron beam exposure.

More precisely, however, we rewrite (8) as

$$N(t) = 2\tau_D/\lambda \quad <V(t)>_{\tau_D} \tag{10}$$

where $<V(t)>_{\tau_D}$ is the velocity averaged over the interval τ_D centered around time t, and is defined in conjunction with eq. 3 by

$$<V(t)>_{\tau_D} = 1/\tau_D \int_{t-\tau_D/2}^{t+\tau_D/2} V(t')dt'$$

$$= 1/\rho c \ell_0 \tau_D \int_{t-\tau_D/2}^{t+\tau_D/2} dt' \int_{L-ct'}^{L-ct'+\ell_0} dx'K(x') \tag{11}$$

(It is understood now that all velocities refer to the rear surface velocity. Also, we have again shifted the time base by the constant value $\tau_D/2$; thus, the fringe count at time $t+t_1 + \tau_D/2$ is related to the average velocity defined by Eq. 11 at time t.) For later purposes it is convenient to define auxiliary variables $x = L-ct$ and $x' = L-ct'$; then Eq. (11) becomes

$$<V(t = L-x/c)>_{\tau_D} = 1/\rho c \ell_0 \ell_D \int_{x-\ell_D/2}^{x+\ell_D/2} dx' \int_{x'}^{x'+\ell_0} dx''K(x'') \tag{12}$$

12

where $\ell_D = c\tau_D$. In this expression the first integral accounts for the velocity averaging in the interval τ_D, the second integral for the finite pulse-width effect, and $K(x)$ accounts for the energy dependence of Γ via Eq. (4). In essence, a record of the fringe count as a function of time is directly related to the velocity history of the rear surface, or more precisely, to the time history of the averaged velocity as expressed by Eqs. (11) or (12).

We now describe how we may extract Grüneisen values from rear surface velocity measurements. Assume for the present that Γ is positive for all energies. Then, experimentally the method reduces to measuring the maximum fringe count observed during the first pass of the stress wave at the rear surface as a function of the initial energy density of the sample and of the incident electron energy dose. That is, we determine

$$N_{max}(E_o, \Delta E_p) = 2\tau_D/\lambda \; \text{Max} \; \{ <V(t)>_{\tau_D} (E_o, \Delta E_p) \}$$

$$= 2\tau_D/\lambda \; V_{max}(E_o, \Delta E_p) \tag{13}$$

where $V_{max}(E_o, \Delta E_p)$ is defined as the maximum <u>averaged</u> velocity observed for the initial specific energy E_o and peak energy deposition ΔE_p. If ℓ_o and ℓ_D are sufficiently small, then we see from Eqs. (12) and (4) that $<V(t)>_{\tau_D}$ achieves its maximum value from that portion of the stress wave generated by the beam heating in the vicinity of x_p, the position of the peak energy deposition. Note that if $\Gamma(E)$ is positive for all $E>E_o$, then the quantity $K(x)$ also achieves its maximum value at the point x_p. Letting t_m be the time that maximizes $<V(t)>_{\tau_D}$ and using Eqs. (12) and (4), we write $V_{max}(E_o, \Delta E_p)$ as

$$V_{max}(E_o, \Delta E_p) = <V(t_m)>_{\tau_D} (E_o, \Delta E_p)$$

$$= 1/\rho c \ell_o \ell_D \int_{x_m - \ell_D/2}^{x_m + \ell_D/2} dx \int_{x}^{x + \ell_o} dx' \int_{E_o}^{E_F(x')} \Gamma(E)dE \tag{14}$$

where $x_m = L - ct_m$. If ℓ_o is much smaller than x_p, which is the case for the present experiments, then the value of x_m depends essentially upon the relative sizes of $\ell_D/2$ and x_p. If $\ell_D/2 < x_p$, then for all practical purposes, x_m coincides with the peak position x_p. On the other hand, if $\ell_D/2 > x_p$, then as a consequence of the symmetry conditions (5), the correct choice of x_m is easily seen to be $\ell_D/2$. That is to say

$$x_m \cong \text{Max} \; \{x_p, \; \ell_D/2\} \tag{15}$$

where the approximately equal sign is used because in principle x_m could be shifted slightly away from the right hand side of (15) due to smoothing effects of the spatial integrations in (14). However, for the work

13

reported here such a shift is entirely negligible. (There could conceivably be a significant shift only if ℓ_o and (or) $\ell_D/2$ are of the order of or greater than the range of the incident electrons in the sample.)

There are several ways one can obtain the energy dependence of Γ from Eqs. 13 and 14. One direct approach, which may be described as an integral (or non-local) method, is simply to expand Γ in a power series in E, retaining as many terms as desired. The expansion coefficients may then be determined by fitting to the measured values of V_{max} (E_o, ΔE_p) in some fashion. Although such a method may be entirely satisfactory, particularly if Γ does not vary too rapidly with energy, we choose to use a differential (or local) method of analysis, which involves expansions of $\Gamma(E)$ only in narrow regions of energy. This method offers the advantage that the errors associated with the expansions of Γ are reduced considerably or, equivalently, only a few terms are needed in the expansion to achieve the same accuracy.

To understand best the motivation for our differential approach, note that in the limits $\ell_o \to 0$ and $\ell_D \to 0$, (14) reduces to

$$V_{max}(E_o, \Delta E_p) = 1/\rho c \int_{E_o}^{E_F} \Gamma(E)dE \qquad (16)$$

where we define $E_F = E_F(x_p) = E_o + \Delta E_p$. (In this case, of course, $x_m = x_p$ and $\Delta E_p = \Delta E(x_p)$). For this limiting case $\Gamma(E)$ can be expressed in terms of $V_{max}(E_o, \Delta E_p) = V_{max}(E_o, E_F)$ in either of two obvious ways, obtained by appropriate differentiation of Eq. 16.

$$(i) \quad \Gamma(E_F) = \rho c \left(\frac{\partial V_{max}}{\partial E_F} \right)_{E_o} \qquad (17a)$$

$$(ii) \quad \Gamma(E_o) = -\rho c \left(\frac{\partial V_{max}}{\partial E_o} \right)_{E_F} \qquad (17b)$$

In other words, we can obtain Γ as a function of energy either by measuring V_{max} as a function of E_F holding the initial energy constant or by measuring V_{max} as a function of E_o holding the final energy constant. In either case $\Gamma(E)$ is determined by the slope of the resulting curve. In addition, we can differentiate (16) with respect to E_o holding ΔE_p constant, obtaining the following relationship

$$(iii) \quad \Gamma(E_o) = \Gamma(E_F) - \rho c \left(\frac{\partial V_{max}}{\partial E_o} \right)_{\Delta E_p} \qquad (17c)$$

In this case $\Gamma(E_o)$ is determined—provided $\Gamma(E_F)$ is known—by measuring V_{max} as a function of E_o holding the energy dose constant.

14

For the case of finite ℓ_O and ℓ_D, matters are not quite this simple, of course, but Eqs. (17) do serve to illustrate the general idea of our procedure. Before discussing the general case, we point out that although in principle each of the three methods is valid for all energies, as a matter of practical convenience they lend themselves to actual analysis of data for different situations. In particular, if Γ is independent of energy, method (i) is the most straightforward to apply; we can simply measure V_{max} as a function of energy dose. (Note that in this case (16) reduces to simply V_{max} (E_O, ΔE_p) = $\Gamma/\rho c\ \Delta E_p$). Method (i) can also be used to determine $\Gamma(E)$ at high energy. Methods (ii) and (iii) are better suited for extracting Grüneisen data in the low energy region. (Keep in mind that in practice ΔE_p is sizeable and can be much greater than E_O). Method (iii) is, of course, restricted for use when Γ values at the final energies are known, whereas method (ii) has no such restriction. However, if $\Gamma(E_F)$ is accurately known, method (iii) offers greater accuracy in applications to be discussed further below.

The procedure we employ for the general case (non-zero ℓ_O and ℓ_D) is as follows. First we write down the expression (14) for V_{max} for two sets of energy parameters (E_O, ΔE_p) and (E_O', $\Delta E_p'$), and then take their difference

$$V_{max}(E_o, \Delta E_p) - V_{max}(E_o', \Delta E_p')$$

$$= (1/\rho c)\left\{ \int_{E_O}^{E_O'} \Gamma(E)dE + \int_{x_m-\ell_D/2}^{x_m+\ell_D/2} \frac{dx}{\ell_D} \int_{x}^{x+\ell_O} \frac{dx'}{\ell_O} \quad (18) \right.$$

$$\left. \int_{E_F'(x')}^{E_F(x')} \Gamma(E)dE \right\}$$

where we have used the fact that the first energy integral is independent of x. (We are setting up the analysis in a completely general way, so that our expressions may be applied to the case of finite increments between the energy parameters as well as to the case of infinitesimal increments. This procedure proves convenient in application to actual data. We can recover the differential expressions generalizing Eqs. (17) by taking appropriate limits). Eq. 18 is exact within linear thermoelastic theory. To proceed further we write the limits of the second energy integral as

$$E_F(x') = E_F - \Delta E_p \ |1-e(x')|$$

$$$$ (19)

$$E_F'(x') = E_F' - \Delta E_p' \ |1-e(x')|$$

where we recall $E_F = E_F(x_p)$. Hence, $e(x)$ is the normalized depth dose profile such that $e(x_p) = 1$, i.e., $e(x) = \Delta E(x)/\Delta E_p$. Next, we expand $\Gamma(E)$ in Taylor series to first order in E around the points $\hat{E}_o = (E_o + E_o')/2$ and $\hat{E}_F = (E_F + E_F')/2$. That is, in the first integral we let

$$\Gamma(E) \approx \Gamma(\hat{E}_o) + \left(\frac{\partial \Gamma}{\partial E}\right)_{E=\hat{E}_F} (E-\hat{E}_F) \tag{20a}$$

and in the second we let

$$\Gamma(E) \cong \Gamma(\hat{E}_F) + \left(\frac{\partial \Gamma}{\partial E}\right)_{E=\hat{E}_F} (E-\hat{E}_F) \tag{20b}$$

These expansions are valid as long as $\Gamma(E)$ is approximately linear in the energy intervals E_o to E_o' and E_F to E_F' and provided that ℓ_o and ℓ_D are small compared with the electron range in the sample—so that $1 - e(x') << 1$ in the range of the spatial integrations of (18). After some straightforward algebra (18) reduces to

$$V_{max}(E_o, \Delta E_p) - V_{max}(E_o', \Delta E_p')$$

$$= 1/\rho c \left\{ \Gamma(\hat{E}_o)(E_o'-E_o) + \Gamma(\hat{E}_F)|E_F-E_F'-(\Delta E_p-\Delta E_p')I_1| \tag{21} \right.$$

$$\left. - \Gamma'(\hat{E}_F)(\Delta E_p+\Delta E_p')/2 \; |(E_F-E_F') \; I_1 - (\Delta E_p-\Delta E_p')I_2| \right\}$$

where

$$\Gamma'(\hat{E}_F) = |\frac{\partial \Gamma}{\partial E}|_{E=\hat{E}_F}$$

and

$$I_n = \int_{x_m-\ell_D/2}^{x_m+\ell_D/2} \frac{dx}{\ell_D} \int_{x}^{x+\ell_o} \frac{dx'}{\ell_o} \; |1-e(x')|^n \tag{22}$$

The factors I_1 and I_2 include the corrections due to both the finite exposure time and the finite delay time. They are independent of the energy parameters E_o, E_o', ΔE_p, $\Delta E_p'$; they depend only upon the values of ℓ_o and ℓ_D and on the shape of the depth dose profile. We note that if ℓ_o and ℓ_D are much less than the electron range, then $I_2 << I_1 << 1$. In fact, for the studies reported here I_2 is entirely negligible. We retain it only for the purpose of keeping our expressions general.

16

Equations (21) and (22) are our basic operating equations. The energy dependence of the Grüneisen parameter is now obtained in a manner similar to the methods indicated by Eqs. 17 for the simplified case of $\ell_o = \ell_D = 0$. We consider each method in turn.

(i) Setting $E_o = E_o'$ in (21) we obtain the equivalent of Eq. (17a)

$$\Gamma(\overset{\curvearrowright}{E}_F) = \rho c \left[\frac{V_{max}(E_o, \Delta E_p) - V_{max}(E_o, \Delta E_p')}{(\Delta E_p - \Delta E_p')(1-I_1)} \right] \tag{23}$$

Taking the limit $E_F - E_F' = \Delta E_p - \Delta E_p' \to 0$, we have

$$\Gamma(E_F) = \frac{\rho c}{1-I_1} \left(\frac{\partial V_{max}}{\partial E_F} \right)_{E_o} \tag{24}$$

As pointed out earlier this method can be used for determining Γ at higher energies. It is particularly useful when Γ is constant for $E > E_o$, in which case (24) becomes

$$\Gamma = \frac{\rho c}{1-I_1} \frac{V_{max}(E_o, \Delta E_p)}{\Delta E_p} \tag{25}$$

(ii) Putting $E_F = E_F'$ in (21) yields

$$\Gamma(\overset{\curvearrowright}{E}_o) = -\rho c \left[\frac{V_{max}(E_o, E_F) - V_{max}(E_o', E_F)}{E_o - E_o'} \right]$$
$$+ \Gamma(E_F)I_1 - \Gamma'(E_F) \left(\frac{\Delta E_p + \Delta E_p'}{2} \right) I_2 \tag{26}$$

which in the limit $E_o' \to E_o$ corresponds to (17b)

$$\Gamma(E_o) = -\rho c \left(\frac{\partial V_{max}}{\partial E_o} \right)_{E_F} + \Gamma(E_F)I_1 - \Gamma'(E_F)\Delta E_p I_2 \tag{27}$$

Hence, if $\Gamma(E)$ is known in the vicinity of E_F we can obtain Γ values at low energy via Eqs. (26) or (27). For the case of finite increments, however, this method may be cast into an alternative form which eliminates the need to know $\Gamma(E_F)$. If instead of setting $E_F' = E_F$ in 21), we choose $E_F' = E_F - (\Delta E_p - \Delta E_p') I_1$, or equivalently, $E_o' = E_o + (\Delta E_p - \Delta E_p') I_1$, we obtain

17

$$\Gamma(\hat{E}_o) = -\rho c \left[\frac{V_{max}(E_o, \Delta E_p) - V_{max}(E_o', \Delta E_p')}{E_o - E_o'} \right] E_o' = E_o$$

$$+ (\Delta E_p - \Delta E_p') I_1 \tag{28}$$

$$+ \Gamma'(\hat{E}_F) \left(\frac{\Delta E_p + \Delta E_p'}{2} \right) \left[\frac{I_1^2 - I_2}{1 - I_1} \right]$$

If ℓ_o and ℓ_D are sufficiently small compared with the electron range, as is the case for our studies, the last term in (28) is small compared with the precision of our results and may be neglected.

(iii) The expression corresponding to (17c) is found by setting $\Delta E_p = \Delta E_p'$ in (21). Noting that $E_o - E_o' = E_F - E_F'$ we have

$$\Gamma(\hat{E}_o) = \Gamma(\hat{E}_F) - \Gamma'(\hat{E}_F) \Delta E_p I_1$$

$$- \rho c \left[\frac{V_{max}(E_o, \Delta E_p) - V_{max}(E_o', \Delta E_p)}{E_o - E_o'} \right] \tag{29}$$

Passing to the limit $E_o' \to E_o$, this becomes

$$\Gamma(E_o) = \Gamma(E_F) - \Gamma'(E_F) \Delta E_p I_1 - \rho c \left(\frac{\partial V_{max}}{\partial E_o} \right) \Delta E_p \tag{30}$$

Again, $\Gamma(\hat{E}_F)$ must be known to evaluate $\Gamma(\hat{E}_o)$.

We note that experimentally it is convenient to present the data for the case where Γ is a function of energy in terms of a family of plots of V_{max} vs E_o for a series of ΔE_p values. If $\Gamma(E_F)$ is unknown—or we prefer not to use it if known—then Eq. 28 with the second term neglected can be used to obtain $\Gamma(\hat{E}_o)$. To minimize the error associated with the expansion of Γ around the point $\hat{E}_o$, adjacent curves (adjacent ΔE_p values) should be used. On the other hand, if $\Gamma(E_F)$ is accurately known, for example, by either method (i) or (ii), then the differential expression (30) of method (iii) can be applied to each plot individually, thereby eliminating the expansion around $\hat{E}_o$. (Note: the differential expression (27) cannot be applied to an individual plot because in using (27) E_F must be maintained constant. We still have an error due to the expansion of Γ around E_F, but in practice Γ generally varies much more slowly at high energy than at low energy, and hence the errors associated with an expansion at high energy are smaller than those associated with an expansion of Γ at low energy. In addition, when ℓ_o and ℓ_D are small the range of the expansion around E_F is correspondingly small, further reducing the error in

18

method (iii). In principle, therefore, method (iii) should provide the most accuracy for temperature measurements, though, of course, Eq. 28 of method (ii) is certainly the most advantageous for use when one wishes to avoid the necessity of knowing Γ at higher energy. We shall apply both methods to reduce the data in the present study.

Up to this point we have been assuming in our discussion that Γ is positive for all values of energy under study. In this case the maximum rear surface velocity results from the stress generated in the vicinity of the peak in the energy deposition profile; the time t_m at which V_{max} is achieved corresponds to the time required for the stress wave to propagate from the position x_m as defined by Eq. 15 to the rear surface, i.e., $t_m = (L - x_m)/c$. (See discussion preceding Eq. 15.) Now we inquire into the situation for which Γ may be negative for certain energy regions under study. This situation is known to be the case for certain materials, for example, the covalent-bonded cubic crystals Si, Ge, and InSb, for which Γ is negative for temperature $T \gtrsim 0.2\ \theta_D$ where θ_D is the Debye temperature of the solid. First, we note that if Γ is in fact negative everywhere in the energy region $E_o < E < E_F$, then our analysis goes through exactly as before, except that the signs associated with the rear surface motion are reversed. The displacement of the rear surface is initially in the negative x direction, and hence V_{max} corresponds to the maximum velocity achieved in the negative direction during the first cycle. Again, V_{max} results from the stress generated in the vicinity $x \sim x_p$.

If Γ changes sign in the interval $E_o < E < E_F$, the velocity in general would not attain its maximum magnitude at the time t_m. Instead, the time at which the velocity is maximum, as well as its sign, depends upon the explicit nature of the energy dependence of Γ and the energy deposition function, and upon the values of E_o and ΔE_p. To avoid causing the analysis to become unduly complicated in determining the values of Γ for this case, we can simply use the fringe count at the time t_m at which the maximum average velocity would occur if Γ were everywhere positive (or everywhere negative). That is, in our analysis we use V_{max} as defined by Eq. 14 where x_m is still chosen by (15); however, we realize that V_{max} so defined may not correspond to the actual maximum rear surface velocity. Of course, we must also take care to ascertain the correct sign of V_{max} in this case. We note, however, that in practice Γ is generally negative only over a relatively small energy interval at low energies—if Γ is negative at all. (Recall that the specific heat of solids at low temperature is proportional to T^3.) Further, the values of ΔE_p that must be used in actual experiments are sufficiently large that the final energy values E_F are rather high in the energy region where Γ is positive. Thus, it turns out that, even when $E_o \sim 0$, the maximum rear surface velocity does in fact usually occur at the time t_m and is positive.

19

III. EXPERIMENTAL PROCEDURE

To establish this Grüneisen parameter measurement technique a series of materials having known Γ values were investigated. Then the values of Γ obtained by applying the analysis described in the previous section to the measured maximum rear surface velocities produced by pulsed electron beam exposure are compared to their thermodynamic values. For the temperature-independent measurements, the materials chosen were Si, Ge, Al, and Cu having a range in Γ from 0.43 to 2.2. The temperature-dependent measurements were carried out on silicon over the range in temperature from 50 to 300°K.

Figure 2 provides a schematic diagram of the experimental arrangement depicting the electron beam, calorimeter, sample and interferometer. The electrons emitted by the field emission tube of the flash x-ray machine stream in a partially evacuated drift tube and emerge through an aperture with a-2 mil titanium transmission window. As previously described[4] this arrangement produces a stable, reproducible electron pulse whose full width at half maximum is approximately 30 nsec with a fluence uniformity of ±10% over the face of the exposed samples. The machine-charging voltage for the exposures reported here was either 4.1 MV or 5.0 MV and produced electron spectra with mean energies of 1.96 MeV and 2.50 MeV, respectively.

The peak energy deposition in the exposed sample was determined using thin, in-line copper calorimeters in the following manner. For measurements of rear-surface velocity at room temperature, the average dose in the calorimeter was measured by the response of a thermocouple welded to the calorimeter. The energy deposition profile in the calorimeter and target material were computed for an incident fluence of one electron/cm^2 using the electron transport code ZEBRA[10] and a measured electron spectrum[4] (also S. Graybill and G. Ames, private communication) corresponding to the operating voltage of the machine. The maximum energy deposition in the target was then determined by multiplying the observed calorimeter response by the predicted ratio of the peak dose in the sample to the average dose in the calorimeter. For the low-temperature measurements with silicon, the calorimeter response at room temperature was normalized to correspond to the peak dose appropriate to the observed peak velocity. Then, for exposures intended to be at a constant fluence, the calorimeter response at lower temperatures was used to determine the constancy of the incident electron fluence while the initial temperature was varied. The initial energy, E_o, was obtained from the measurement of the initial temperature using the Debye specific heat with a Debye temperature of 650°K.

The target sample, calorimeter and optics were supported on a vibration isolation table independent of the electron beam machine. All the samples used were optically polished with flat and parallel faces. For the room temperature measurements the samples were disks that had a diameter of 5.08 cm and a mass thickness approximately 1.1 g/cm^2. These samples were mounted by supporting the sample around its edge with a

20

neoprene O-ring which applied a slight pressure. Under this arrangement
the exposed diameter to thickness ratio was greater than 10 to 1 for all
the samples exposed for the room temperature measurements. For the cry-
ogenic exposure of silicon, the samples were rectangular slabs that were
glued to the cold finger of a variable temperature liquid helium Dewar
flask as previously described[5]. The cold finger had an aperture to permit
observation of the rear surface motion of the sample. To insure that the
effects of the constraints caused by bonding the sample to the cold finger
would not be observed during the first half cycle of the induced motion,
the diameter of the aperture was made greater than twice the thickness of
the sample. Thus for both the temperature independent and temperature
dependent measurements the observed response could be considered to be
one-dimensional for at least the first half cycle of motion.

The rear-surface velocity of the exposed samples was measured using
a velocity interferometer similar to the type developed by Barker.[7]
The interferometer employed a collimated, single-mode, 6328Å, He-Ne laser
as the light source. The laser beam was directed through a lens which
focused the beam onto the rear surface of the sample where it was re-
flected along a separate return path and recollimated by a second lens.
The rear-surface velocity of the target was determined by the Doppler
shift in frequency in the reflected laser beam. The frequency shift
was measured with a Mach-Zender interferometer composed of the beam
splitter and two retroreflectors. The Doppler shift is detected through
the interference fringes of the recombined beams as described in Section
II. The fringes were detected with a RCA Type 7265 photomultiplier tube,
whose output was amplified using a wide band amplifier having a fixed
gain of 20 dB over the frequency range from 200 Hz to 200 MHz. This
signal was recorded on an oscilloscope. The combined rise time of the
photomultiplier, amplifier and oscilloscope was approximately 12 nsec.
The maximum "averaged" rear surface velocity was obtained from the re-
corded interferometer trace by determining the maximum fringe count
(occurring at time t_m) and using the velocity interferometer relation-
ship given T_L Eq. 10. For the measurements reported here, the difference
in optical path lengths was varied between 8 and 52 m with corresponding
delay times ranging from 26 nsec to 170 nsec.

IV. RESULTS

A. Energy-Independent Grüneisen Measurements

To verify the experimental technique, the Grüneisen values for Si,
Ge, Cu and Al (6061) were determined over an energy interval where Γ is
constant using Eq. 25. The results were compared with thermodynamic
values reported in the literature.[11,12] For these measurements the
values of V_{max} (ΔE_p), ΔE_p, and the acoustic speed c were determined
experimentally; widely published values were used for the densities.
The correction term I_1 for the effect of finite pulse width and inter-
ferometer delay time was computed in accordance with Eqs. 22 and 15
using the measured values of τ_0 (= 30 nsec) and τ_D along with the

[11] Karl A. Gschneidner, Jr., in Solid State Physics, edited by F. Seitz
and D. Turnbull (Academic Press, New York, 1970), Vol. 16, p. 410.
[12] K. Brugger and T. C. Fritz, Phys. Rev. 157, 525 (1967).

21

computed deposition profile based upon the measured electron spectrum.
(See fig. 1 for aluminum.) V_{max} was measured as a function of the peak
dose deposited in the material; these peak doses ranged from a minimum
of 3×10^8 ergs/cm^3 to a maximum of $12 - 45 \times 10^8$ ergs/cm^3 depending
upon the material. Typical results for these measurements are shown
for Al in figure 3. By fitting a straight line to the V_{max} vs ΔE_p data,
the errors in both the dosimetry and velocity measurements are reduced
through an effective averaging process. The acoustic speed of each
material was determined simultaneously with the measurement of V_{max} by
observing the time required for the stress pulse to propagate twice
through the sample and then combining this "round trip" time with the
measured thickness of the sample.

Results are shown in Table I. In all cases, the observed values
of Γ are within approximately 5% of the tabulated thermal values. In
fact, except for Al there is agreement within 2%. However, the samples
used in the present experiments were not pure Al but were made from the
aluminum alloy 6061 (1.0% Mg, 0.6% Si, 0.25% Cu, 0.25% Cr, 97.9% Al).

B. Energy-Dependent Grüneisen Measurements

The changes in the free surface velocity of silicon resulting from
the variation of Γ with specific energy, or temperature, are illustrated
in Figures 4a and 4b. These figures show the velocity interferometer
traces for a Si single-crystal sample oriented with the |100| axis
parallel to the incident electron flux exposed to receive a peak dose
of 10.7×10^8 ergs/cm^3 but at two initial specific energies 1.73×10^8
and 16.5×10^8 ergs/cm^3. At an initial energy of 16.5×10^8 ergs/cm^3
($T_0 = 244°K$), $\Gamma(E)$ is very near its high energy limit of 0.43; thus the
electron-beam exposure produces a velocity history which is character-
istic of the constant high temperature value for Γ. As indicated in
figure 4a the peak velocity corresponds to a fringe count of 2.2 at 680
nsec. A marked decrease in velocity is produced by lowering the initial
energy to 1.73×10^8 ergs/cm^3 ($T_0 = 108°K$) while maintaining the same
peak dose. As shown in figure 4b, the peak velocity to correspond to
a fringe count of 1.0. The decrease is the direct result of the re-
duction in Γ at lower specific energy.

The effects produced on the measured velocity history by varying
the initial energy is shown more explicitly in figure 5. In these plots
we show the velocity histories as obtained directly from the inter-
ferometer traces, again for the 100 orientation and for a constant peak
deposition of 11.1×10^8 ergs/cm^3. Therefore, they are the "averaged"
free surface velocities as described by Eq. 11; they include the effect
of the long risetime of the interferometer due to the large optical
delay time ($\tau_D = 170$ nsec) used for these measurements. The solid lines
in figure 5 are drawn to fit the experimental data. Two effects are
observed as the initial temperature is decreased: (1) a decrease in
velocity at lower temperatures, and, (2) changes in the velocity profile,
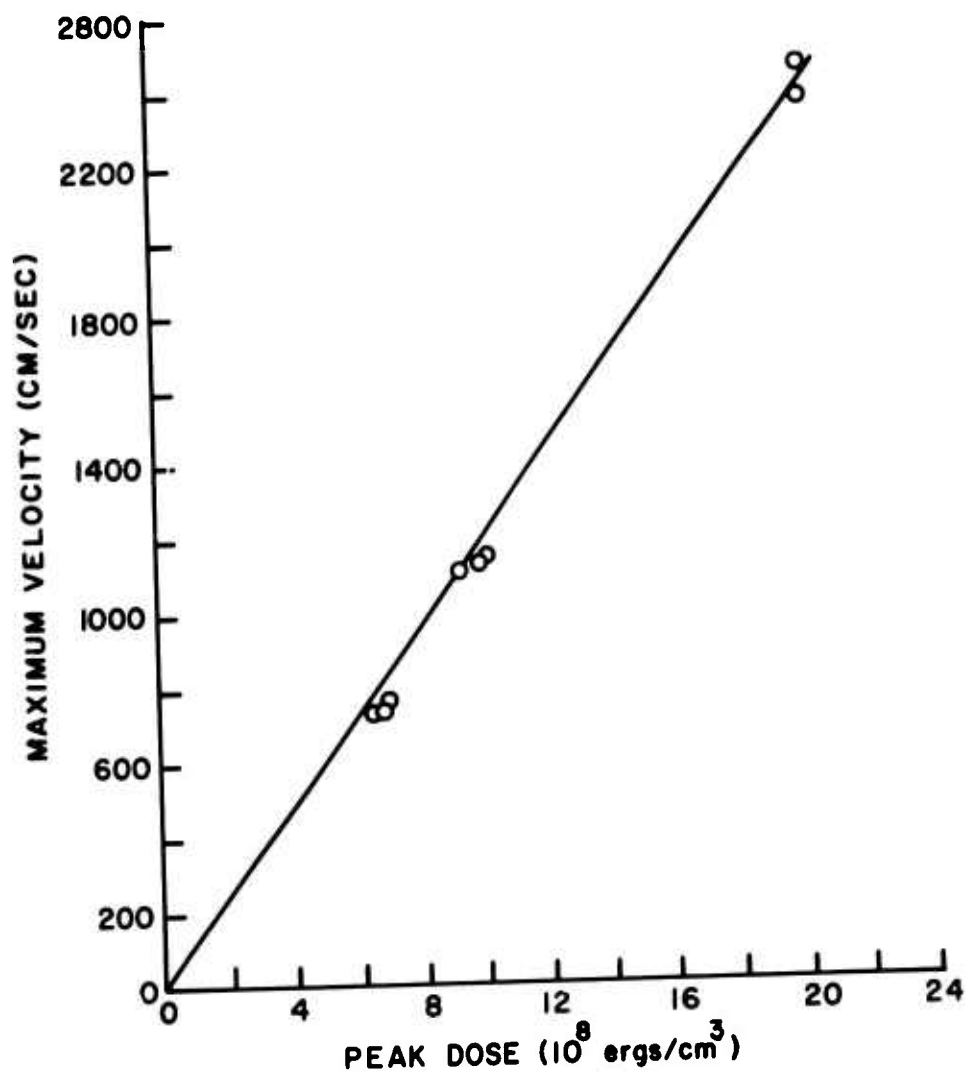particularly over the early portion of the history. This change in

22

Figure 3. Measured peak velocity vs. peak dose, ΔE_p, for aluminum 6061 exposed to the pulsed 1.96 MeV electron beam at room temperature.

Table I. Comparison of Measured Values of Γ with
Tabulated Thermodynamic Values of Γ from
the Literature.

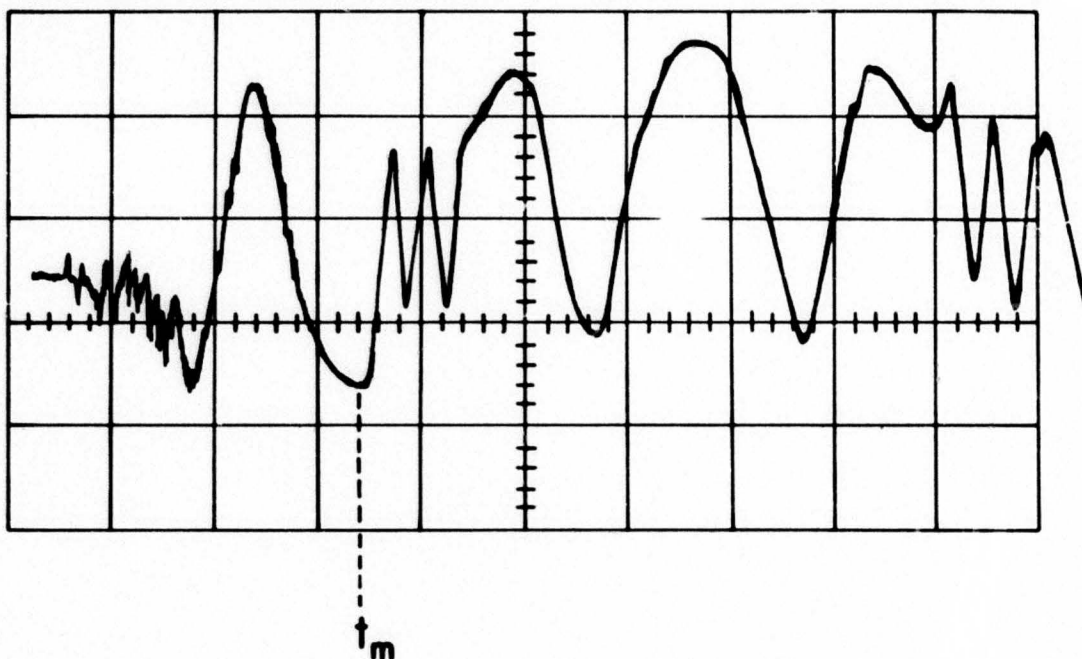| Material	c (10^5 cm/sec)	τ_D(nsec)	I_1	Γ^{meas}	$\Gamma^{thermal}$
Si [111]	9.36	170	.047	.42	.43
Ge [111]	5.95	42	.014	.75	.76
Al (6061)	6.67	42	.006	2.07	2.17
Cu	4.87	26	.015	2.00	2.00

t_m

Figure 4a. Velocity interferometer traces for a Si single crystal
exposed with the [100] axis oriented parallel to the
direction of the incident electron beam. Both traces
correspond to a peak energy deposition of 10.7 x 10^8
ergs/cm^3 but at initial temperatures of (a) T_o = 244°K
and (b) T_o = 108°K. The horizontal and vertical scales
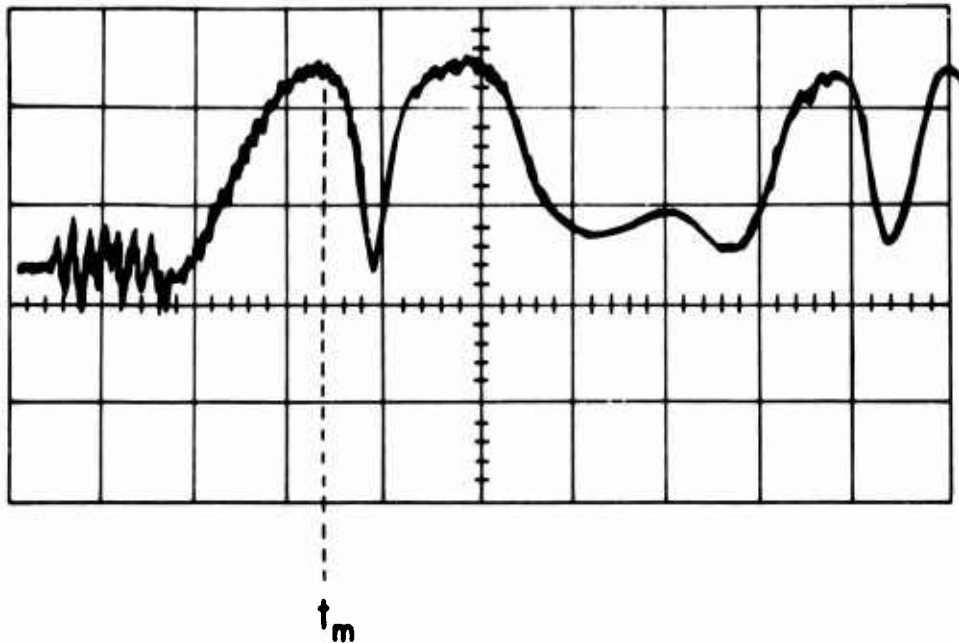are 200 nsec/major division and 0.20V/major division,
respectively.

t_m

Figure 4b. Velocity interferometer traces for a Si single crystal
exposed with the |100| axis oriented parallel to the
direction of the incident electron beam. Both traces
correspond to a peak energy deposition of 10.7 x 10^{8}
ergs/cm^{3} but at initial temperatures of (a) T_o = 244°K
and (b) T_o = 108°K. The horizontal and vertical scales
are 200 nsec/major division and 0.20V/major division,
respectively.

shape results from the fact that each portion of the velocity history
corresponds to an integral of $\Gamma(E)$ over different energy intervals, as
can be seen by referring to Eqs. 4 and 12. Therefore, unless $\Gamma(E)$ is
constant over the energy intervals of interest, the changes in the
velocity history with temperature should in general be non-linear.
The velocity curves of figure 5 show evidence of such non-linear behavior
for Si over the specific energy interval from 1 x 10^{8} to 20 x 10^{8} ergs/
cm[3]. The dashed curves in figure 5 are the corresponding velocity
histories calculated from Eq. 12 using the energy dependent $\Gamma(E)$ as de-
termined from our measurements. These curves will be discussed in
further detail below.

To demonstrate the use of the analysis developed in Section II for
determining an energy-dependent $\Gamma(E)$, the Grüneisen parameter of Si was
measured over a range in initial energy density from 1 x 10^{8} to 24 x 10^{8}
ergs/cm^{3} and then compared with thermodynamic data[13,14]. For these
measurements single crystal samples with |111| orientation were used.

[13]D. F. Gibbons, Phys, Rev. 112, 136 (1958).
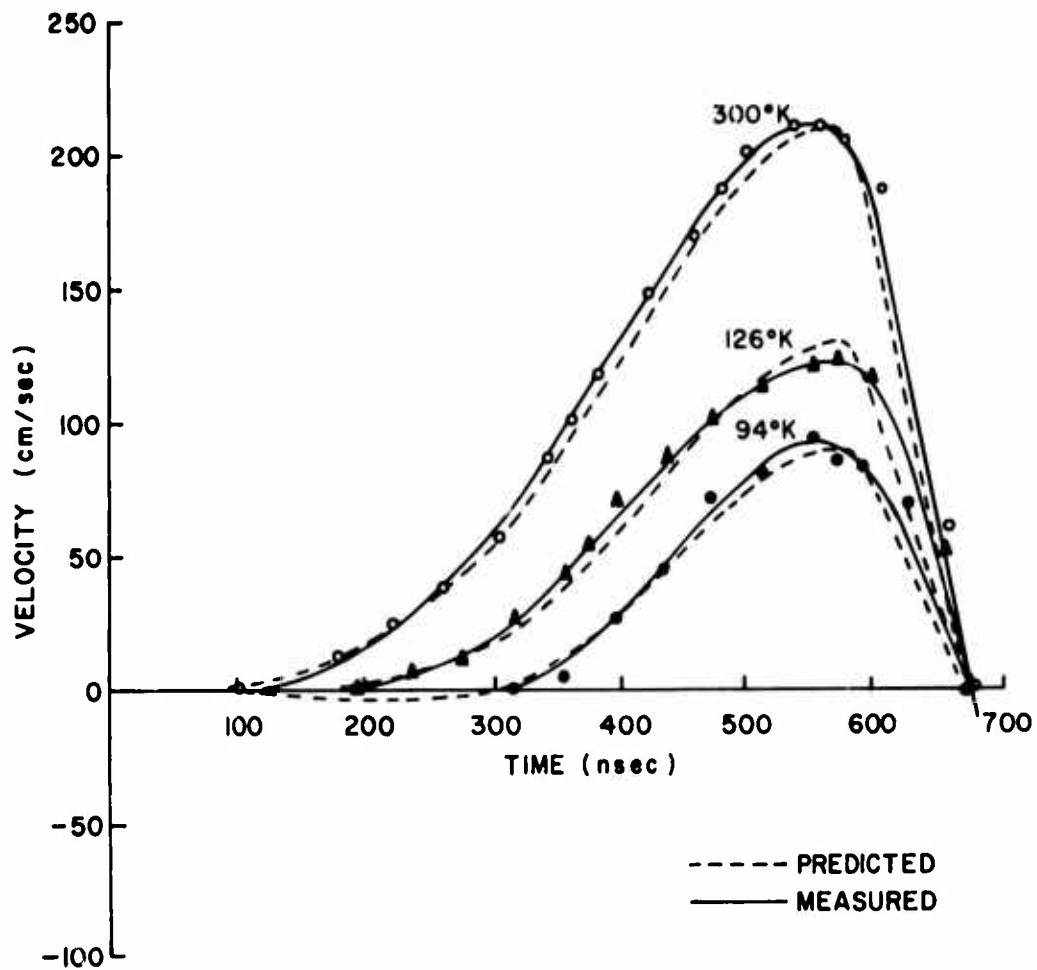[14]R. H. Carr, R. D. McCammon, and G. H. White, Phil. Mag 12, 157 (1965).

Figure 5. Comparison of measured and calculated velocity histories
corresponding to the response of a single crystal of Si
oriented with the [100] axis parallel to the direction of
the incident electron beam and at three different initial
temperatures (a) $273^{\circ}K$, (b) $126^{\circ}K$ and (c) $94^{\circ}K$. The
solid curves are drawn to fit the data points; the dashed
curves are computed from Eq. 14 using our measured energy-
dependent Γ.

First, we used Eq. 28 of method (ii) with the last term omitted to obtain
$\Gamma(E)$, in which case it is not necessary to use Grüneisen values for higher
energy. Then these results were used in conjunction with Eq. 30 (method
iii)) to obtain a more reliable estimate of $\Gamma(E)$ at lower energy densities.
The values used for V_{max} (E_O, ΔE_p) were determined in the following manner.
Maintaining the peak dose at a constant value, the maximum rear surface
velocity was measured at several initial specific energy values covering

the range from 1×10^8 to 24×10^8 ergs/cm^3. These data were then fitted with a smooth curve thereby giving V_{max} (E_o, ΔE_p) vs E_o for the fixed value of ΔE_p. Again, the fitting of a smooth curve to the data effectively averages out experimental errors associated with dosimetry and with reading the maximum fringe counts. The procedure was repeated for six different peak doses as shown by the family of plots in figure 6—those in figure 6a were obtained with the 1.96 MeV electron beam and those in figure 6b with the 2.5 MeV beam. This family of curves formed the data base used in the analysis. For the analysis ρ and c were assumed to be constant and equal to their room-temperature values. Again, the value of I_1 was determined from the values of τ_o and τ_D ($\tau_o = 30$ nsec and $\tau_D = 170$ nsec) and from the computed deposition profiles. For the 1.96 MeV beam $I_1 = .047$ and for the 2.5 MeV beam $I_1 = .028$. (The value of I_2 is of the order of .001 in both cases; hence, the second term of Eq. 28 is completely negligible.)
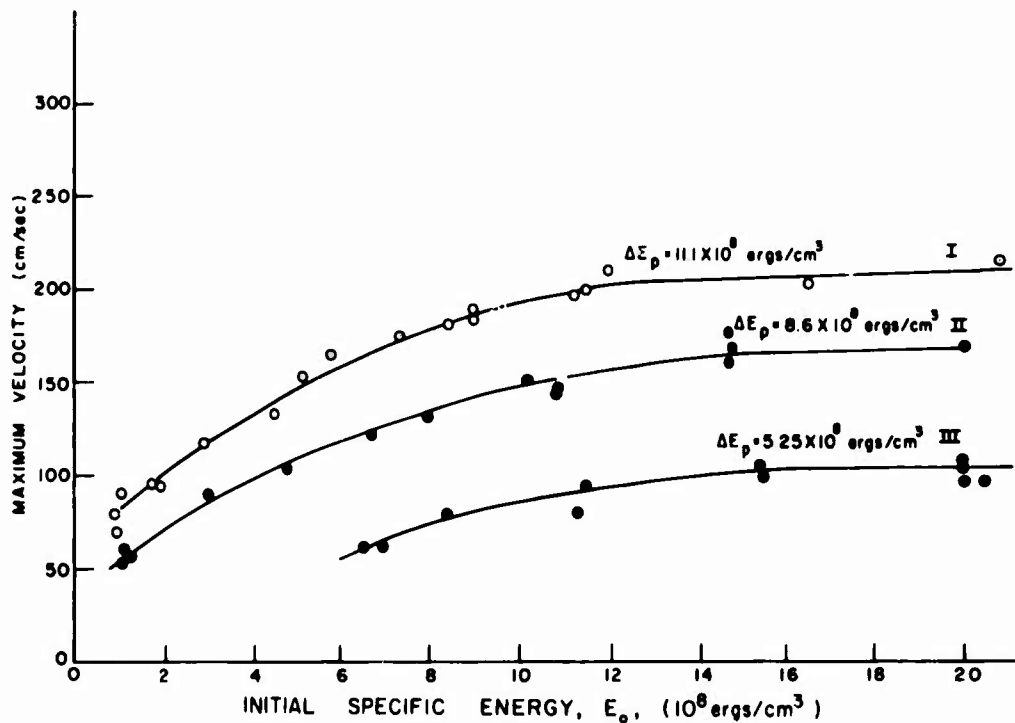

Figure 6a. Maximum velocity vs. initial energy for silicon single crystal samples with |111| orientation exposed to six values of peak deposition ΔE_p. The curves in (a) were obtained with the 1.96 MeV electron beam and those in (b) with the 2.5 MeV beam.
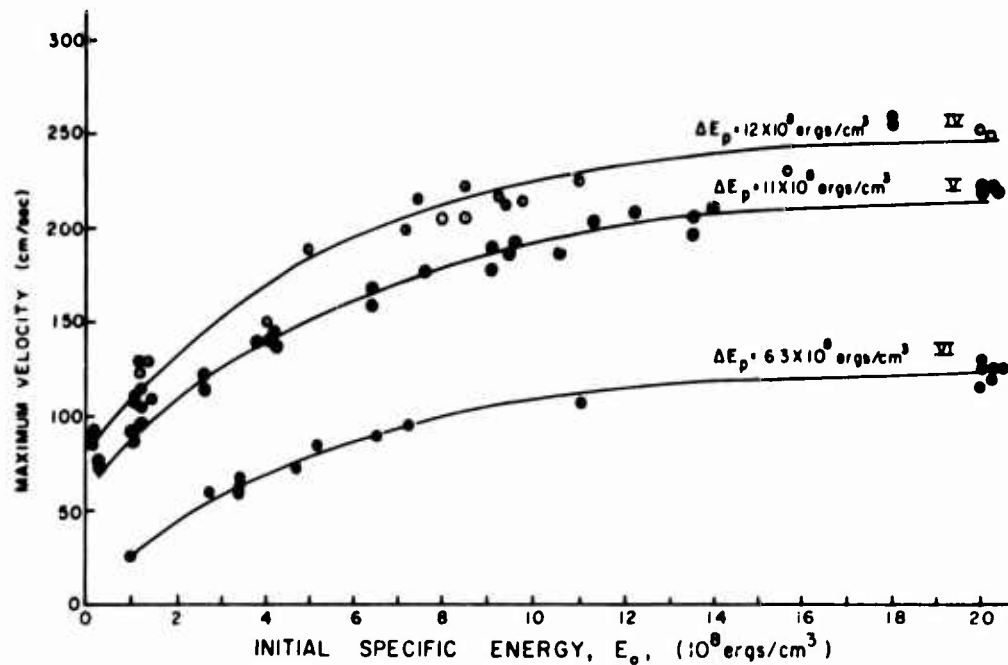
27

Figure 6b. Maximum velocity vs. initial energy for silicon single
crystal samples with |111| orientation exposed to six
values of peak deposition ΔE_p. The curves in (a) were
obtained with the 1.96 MeV electron beam and those in
(b) with the 2.5 MeV beam.

In figure 7 we present the results for Γ vs E using Eq. 28. To
minimize the error associated with the expansion of $\Gamma(E)$ around the
point $\bar{E}_o = 1/2 \ (E_o + E_o')$, we used only adjacent V_{max} curves (for the
same electron spectrum) in obtaining the differences $V_{max} |(E_o, \Delta E_p)$
$- V_{max} \ (E_o', \Delta E_p')|$. More explicitly, for given (adjacent) values of
ΔE_p and $\Delta E_p'$, a value of E_o is chosen and the corresponding value of
$V_{max} \ (E_o, \Delta E_p)$ is read from the experimental curve (fig. 6). Then
$V_{max} \ (E_o', \Delta E_p')$ is found from the $\Delta E_p'$ curve at a value of E_o' such
that the requirement $E_o' = E_o + (\Delta E_p - \Delta E_p') \ I_1$ is fulfilled. Then
application of (28) yields $\Gamma(\bar{E}_o)$. This procedure was iterated over
the entire range of possible $\bar{E}_o$. In figure 7 each of the four symbols
represents data obtained from a pair of adjacent velocity curves. A
visual-inspection "best fit" curve (solid line) drawn through the
resulting data then represents our experimentally determined ene j
dependent $\Gamma(E)$. For purposes of comparison the thermal data of
Gibbons[13] and Carr,[14] et al (dashed curve) is also shown in figure 7.
As can be seen there is reasonably good agreement between our
measured $\Gamma(E)$ and the thermal data for all energy, the agreement
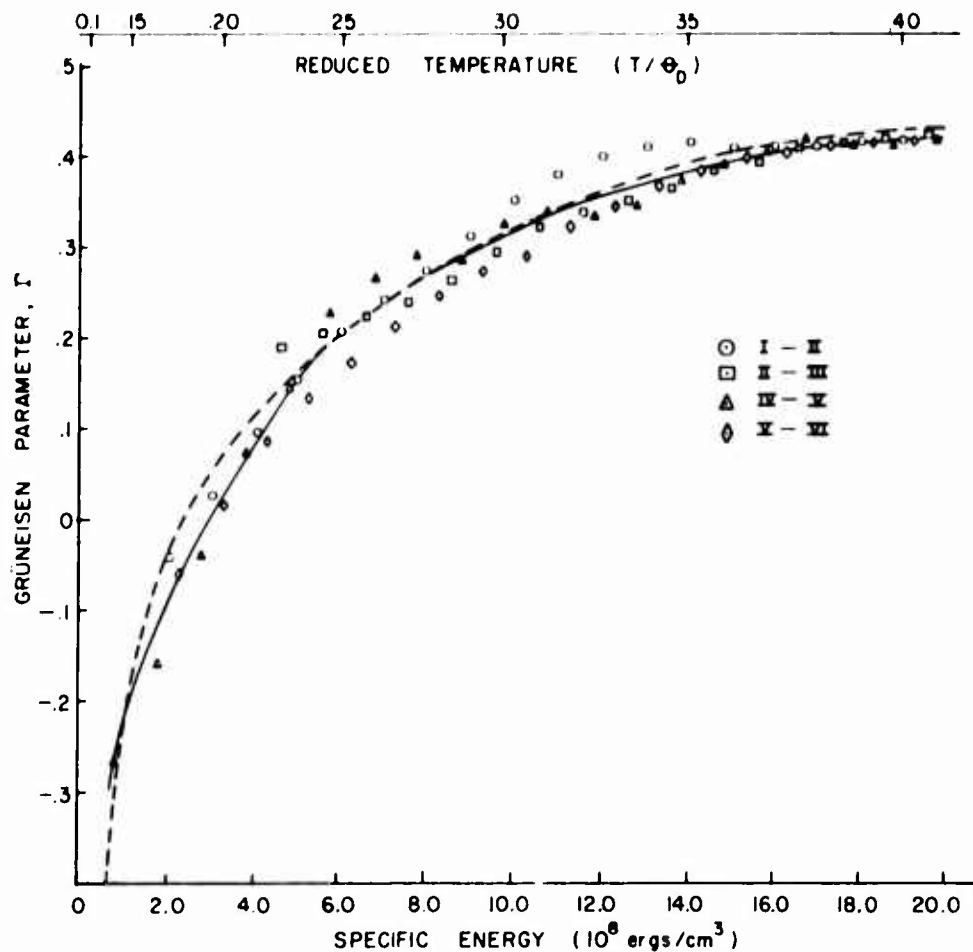
28

Figure 7. Measured values of Γ vs specific energy for silicon ob-
tained by applying Eq. 28 (method ii) to the data base
of figure 6. The data points correspond to pairs of
adjacent plots in figure 6. The solid curve is a best
fit to the data points, and the dashed curve represents
the thermodynamic values of Γ(E) after D. . Gibbons[13]
and R.F. Carr, et al[14].

being very close at high energy but less so at lower energy. That the
agreement is less satisfactory at low energy and that the measured curve
lies below the thermodynamic curve (except at the lowest energies where
there are probably large errors in measuring the initial temperatures)
is not totally unexpected. As discussed in section I , by using method
(ii) we are approximating Γ(E) in the range E_o to E_o' with a linear curve.

In the first place, $\Gamma(E)$ varies most rapidly with E at low energy and such an approximation is expected to be poorer in this region than at high energy. Secondly, when we approximate a nonlinear curve with straight line segments the resulting approximate curve will lie to the concave side of the exact curve.

To improve our measurement of $\Gamma(E)$, particularly at lower energy, we used the differential expression (30) in conjunction with the above results from method (ii) for $\Gamma(E)$ at higher energy. In this case the analysis was applied to each experimental curve in figure 6 individually. The value of Γ at a point E_0 was determined from the slope of the maximum velocity curve at E_0 together with the linear fit to Γ at $E_F = E_0 + \Delta E_p$ in accordance with (20b). The data points (up to six) for each value of E_0 were then averaged with the results shown in figure 8. Here, the error bars reflect the statistical uncertainty (not experimental error) associated with each value of E_0. Again, we compare with the thermal data (dashed curve). As is apparent the agreement is significantly improved at lower energy; there is essentially exact agreement for $E > 2 \times 10^8$ ergs/cm^3. The large discrepancies at the very low energies are probably due to rather large errors in the initial temperature measurement. One point of note is that we are quite definitely measuring negative Grüneisen values for $E < 2.4 \times 10^8$ ergs/cm^3. Thus, our technique is fully capable of handling this region even though the final energy densities lie well up into the region where Γ is positive.

As a final check on our measurements we compute the velocity time histories corresponding to the observed ones in figure 5 using Eq. 12 and the measured $\Gamma(E)$ curve of figure 8. The results are the dashed curves in figure 5. We consider the agreement entirely satisfactory. It demonstrates the validity of the thermoelastic model which forms the basis for Eq. 12 as well as the reliability of our technique for determining $\Gamma(E)$. We note that the computed velocity history for $T_0 = 94°K$ contains an initial negative velocity region corresponding to the fact that the integral over $\Gamma(E)$ is negative in the tail of the energy deposition profile. As T_0 is lowered even further this negative velocity region increases both in magnitude and in extent in time.

V. DISCUSSION

The results presented in this paper demonstrate that the free surface velocity of a thermoelastic solid subjected to pulsed energy deposition can be used to determine both energy-dependent as well as energy-independent Grüneisen data. The experimental results further demonstrate the adequacy of the model of thermoelastic response to account for the effects of the finite pulse width of the electron beam and the finite rise time of the velocity interferometer used.

This technique provides a complementary procedure to those using propagated stress or free surface displacement to measure Γ. In a previous paper[5] a technique was outlined (but not utilized) to measure
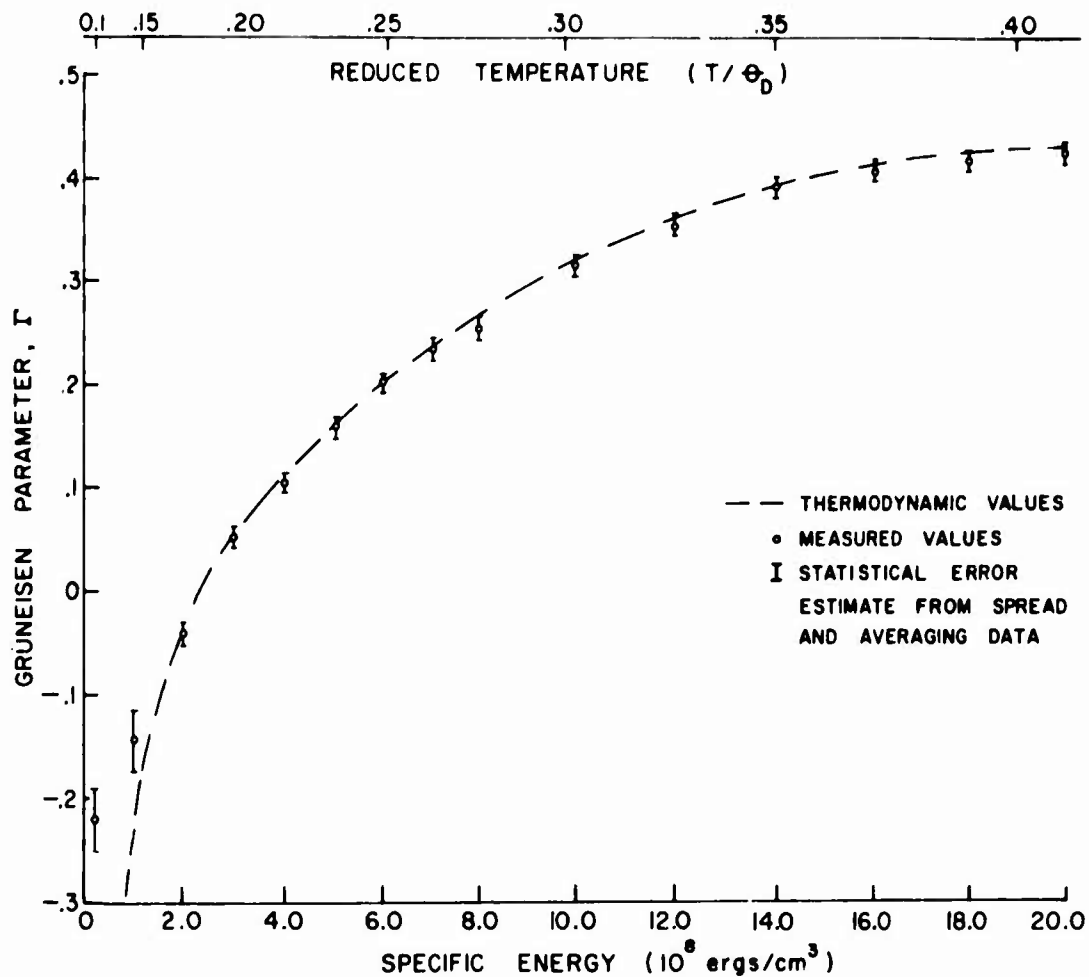
30

Figure 8. Measured energy dependence of Γ for silicon obtained by
applying the differential expression (30) (method iii) to
the data of figure 6 and using the measured Γ(E) values
shown in figure 7 for the final energy densities E_F.
The error bars reflect the statistical uncertainty of
averaging the data. The thermodynamic energy dependence
of Γ is given by the dashed curve.[13,14]

the temperature dependence of Γ using a Michelson interferometer. How-
ever, the free surface velocity is related to Γ(E) through a single
integral over energy while the free surface displacement is related to
Γ(E) through a double integral (a spatial integral over the whole of the
deposition region in addition to the energy integral). Therefore, Γ(E)
was determined from free-surface velocity rather than displacement
measurements.[13]

31

As transmitted stress is also related to Γ via a single integral, the use of stress measurements as a function of initial temperature is also an applicable technique for measuring $\Gamma(E)$. Recently, Gauster[6] performed such measurements in aluminum and silicon using quartz gauge-pressure transducers bonded to the samples. The quartz gauge measurements offer the advantage that low stress levels can be measured, and hence low electron fluences can be used with correspondingly small temperature rises in the samples. However, relatively large-diameter gauges must be used to achieve sufficient accuracy at low stress levels, and this may lead to difficulty with short one-dimensional read times. On the other hand, with the velocity interferometer one can measure the response at a point in the center of the sample rear surface and therefore enjoy the full one-dimensional read time as determined by the acoustic speed and the ratio of the beam area to the sample thickness. For many high-fluence electron beam facilities currently available, the beam area is typically 3 cm^2. Thus, for a low density material, with a small Grüneisen parameter and low acoustic speed the longer read time attainable with the velocity interferometer may be advantageous. This advantage is particularly important for those cases where there is appreciable attenuation of the stress pulses as they propagate through the sample. For exposures below the spall threshold, it is possible with interferometric techniques to observe the motion of the rear surface over several cycles and correct for the attenuation[4]. An additional advantage of the velocity interferometer is that it does not require the presence of a second material medium to measure the response. For high temperature studies, the need for the second material may introduce problems associated with the bonding of the quartz gauges to the samples.

Additional measurements of energy-independent Γ values have been carried out with 750 and 200 KeV electron beams producing peak doses greater than 10^{10} ergs/cm^3, thus enabling the use of velocity interferometers with delay times of 6 nsec and less. These results were equally successful in demonstrating the utility of this procedure.

The precision of an individual measurement in the velocity interferometer technique is limited by the errors in dosimetry and measured velocity. The precision of the dosimetry technique is within approximately ±10%, while the fringe count can be read to within approximately a tenth of a fringe. Hence, the precision of the velocity measurement is ±0.1 ($\lambda/2\tau_D$). Thus for a fixed delay time the relative error increases as the velocity decreases. For both the energy-independent and energy-dependent measurements the maximum velocity values used in the analysis were determined from smooth curves fitted to the data, giving V_{max} in the first case as a function of peak dose in the second case as a function of initial energy density. In addition, for the energy-dependent measurements the results of several experimental runs were averaged to produce $\Gamma(E)$ at each value of E. In this manner the random errors in the data are effectively averaged out to a great extent,

thereby improving the accuracy of our measured values of Γ. As we have seen, our measured values of Γ all lie with 5% of the thermodynamic values, except for the low energy region in the temperature-dependent results for silicon, where a relatively large constant error in the initial temperature measurement at the lower temperatures is probably responsible for the discrepancy.

LITERATURE CITED

1. R.B. Oswald, Jr., D.R. Schallhorn, H.A. Eisen, and F.B. McLean, Appl. Phys. Letters 13, 270 (1968).

2. R.B. Oswald, Jr., F.B. McLean, D.R. Schallhorn, and L.D. Buxton, Appl. Phys. Letters 16, 24 (1970).

3. R.A. Graham and R.E. Hutchison, Appl. Phys. Letters 11, 69 (1967).

4. R.B. Oswald, Jr., F.B. McLean, D.R. Schallhorn and L.D. Buxton, J. Appl. Phys. 42, 3463 (1971).

5. F.B. McLean, R.B. Oswald, Jr., D.R. Schallhorn and L.D. Buxton, J. Appl. Phys. 42, 3474 (1971).

6. W.B. Gauster, Phys. Rev. B 4, 1288 (1971).

7. L. Barker, Behavior of Dense Media Under High Dynamic Pressure, Symposium HDP IUTAM, Paris, 1967, Gordon and Breach, New York, N.Y. p. 483 (1968).

8. W.B. Gauster, Phys. Rev. 187, 1035 (1969).

9. R.J. Clifton, J. Appl. Phys. 41, 5335 (1970).

10. M.J. Berger, in Methods in Computational Physics, edited by B. Alder, et al (Academic Press, New York, 1963), Vol. 1, p. 135.

11. Karl A. Gschneidner, Jr., in Solid State Physics, edited by F. Seitz and D. Turnbull (Academic Press, New York, 1970), Vol. 16, p. 410.

12. K. Brugger and T.C. Fritz, Phys. Rev. 157, 525 (1967).

13. D.F. Gibbons, Phys. Rev. 112, 136 (1958).

14. R.H. Carr, R.D. McCammon, and G.H. White, Phil. Mag 12, 157 (1965).